



Influence of ion size effects on the electrokinetics of aqueous salt-free colloids in alternating electric fields

F. Carrique  and E. Ruiz-Reina *Departamento de Física Aplicada II, Facultad de Ciencias Universidad de Málaga, 29071 Málaga, Spain*F. J. Arroyo *Departamento de Física, Facultad de Ciencias Experimentales Universidad de Jaén, 23071 Jaén, Spain*A. V. Delgado *Departamento de Física Aplicada, Facultad de Ciencias Universidad de Granada, 18071 Granada, Spain*

(Received 8 July 2020; accepted 31 August 2020; published 24 September 2020)

Electrokinetics is the science of the physical phenomena appearing at the solid-liquid interface of dispersed particles subjected to external fields. Techniques based on electrokinetic phenomena constitute an important set of tools for the electrical characterization of colloids because of their sensitivity to the properties of particle-solution interfaces. Their rigorous description may require inclusion of the effects of finite size of chemical species in the theoretical models, and, particularly in the case of salt-free (no external salt added) aqueous colloids, also consideration of water dissociation and possible carbon dioxide contamination in the aqueous solution. A new ac electrokinetic model is presented for concentrated salt-free spherical colloids for arbitrary characteristics of the particles and aqueous solution, including finite-size effects of chemical species by appropriate modifications of the chemical reaction equations to include such non-ideal aspects. The numerical solution of the electrokinetic equations in an alternating electric field has also been carried out by using a realistic non-equilibrium scenario accounting for association-dissociation processes in the chemical reactions. The results demonstrate the importance of including finite-size effects in the electrokinetic response of the colloid, mainly at high frequencies of the electric field, and for highly charged colloids. Findings of previous models for pointlike ions or for ideal salt-free colloids including finite ion size effects are recovered with the present model, for the appropriate limiting conditions.

DOI: [10.1103/PhysRevE.102.032614](https://doi.org/10.1103/PhysRevE.102.032614)

I. INTRODUCTION

For more than a century, a great effort has been devoted to the control and understanding of the response of systems composed of small charged particles dispersed in aqueous or nonaqueous solutions subjected to electric fields [1–4]. This is the realm of the electrophoresis of colloids (particles from micro- to nanoscale in size) and innumerable experimental and theoretical studies have been developed to characterize and predict their behavior. In particular, recent advances in nanomedicine with the use of functionalized nanoparticles as transport vehicles for controlled drug delivery and release [5–9], or the attempts of modeling the electrokinetic behavior and physicochemical properties of viruses, bacteria, living cells, proteins, DNA, and RNA, etc., have stimulated a renewed interest in these systems [10,11]. It is well known that electrophoretic techniques constitute valuable tools for the characterization of such systems. Specially, the frequency response of the colloids to an alternating electric field provides a great deal of information on the dynamics of the electric double layers (EDLs) surrounding the particles in the solution, due to its sensitivity to the electrical particle-solution interface characteristics. These electric double layers govern most of the electrokinetic properties of charged complex fluids, and

improving its knowledge is essential for the development of new applications.

However, there is a special kind of colloids which has attracted the interest of scientists in recent years. They are known as salt-free colloids [3,12,13]. These systems are composed of charged particles and the exact countercharge released by the particles to the solution (the so-called “added counterions”), thus preserving electroneutrality. Salt-free colloids can form crystals or glasses at relatively low particle volume fractions, as the repulsive electrical particle-particle interactions are less screened in comparison with the situation in electrolyte solutions at typical ionic strengths [14–16].

Likewise, most of the industrial applications are related to concentrated rather than dilute colloids. For that reason, in the past decades a huge effort has been focused on the development of theoretical models to account for the electrokinetic and general transport properties of these concentrated systems [17–20]. Unfortunately, the theoretical problems increase with particle concentration due to the enhancement of electrohydrodynamic particle-particle interactions which hamper the mathematical treatment to a large extent, commonly preventing rigorous approaches. In this sense, the use of mean-field models based on average considerations of fields and interactions is a common tool to address this problem. Apart

from different attempts concerning microscopic descriptions of these systems, which consider particle-particle correlations explicitly [21,22], the above-mentioned use of average approaches is still highly demanded. Thus, mean-field approximations, like the cell model [23–27], based on the classical Poisson-Boltzmann (PB) equation, hence on the assumption of pointlike ions, have been profusely used for the theoretical equilibrium description of the ionic populations in the colloid, even for the concentrated particle range, prior to address its response to external electric fields.

In this work a particular aspect beyond the standard PB approach for pointlike species will be taken into account. A nonideality linked to the finite size of species in the aqueous solution will be considered in the theoretical analysis. Excluded volume effects have been widely dealt with in recent literature, and have shown that accounting for the ion size is essential for a proper description of the concentration of species around the nanoparticles, and therefore, for the understanding of their rheological and electrokinetic behavior, mainly for highly charged nanoparticles [28–32]. For example, when ion size effects are considered, a huge magnification has recently been predicted of the high frequency dielectric relaxation process of the condensate layer of counterions that develops in a region close to the particle surface in highly charged colloids [27,33].

Turning back to the salt-free concentrated colloids, the majority of studies refer to dispersed particles in aqueous solutions, and most of them correspond to dispersions open to the atmosphere. These two facts have been considered in previous works, as ions stemming from water dissociation, and additional species originated from the contamination by atmospheric carbon dioxide dissolved in the solution, make the salt-free colloid to behave as a low-salt colloid, or a “realistic salt-free colloid,” hereafter. These aspects have been shown to be crucial for the electrokinetic response in *dc* and *ac* electric fields [20]; for instance, a remarkable decrease has been found of the *dc* electrophoretic mobility as a consequence of the larger screening effect of particle charge in realistic conditions. Also, it has been shown that the low-frequency dependence of the *ac* electrophoretic mobility or the electric permittivity of the colloid can be quite different for realistic and pure salt-free systems [33].

In this contribution we describe the *ac* electrokinetics of a salt-free colloid with arbitrary particle concentration and surface charge in a realistic aqueous solution. This will be addressed by using a mean-field approach based on the cell model concept, with the inclusion of finite-size effects of the species, either neutral or charged, in the solution, with the exception of water molecules (water will be considered as a continuous pure solvent). The basic assumption of the cell concept is that the properties of the full colloid can be derived by proper averages in the ambit of a unit cell that represents a portion of the colloid that includes one particle and its surroundings. The outer radius of the cell is typically chosen by matching the particle volume fraction of the cell with that of the full colloid. The electrohydrodynamic particle-particle interactions are described by appropriate boundary conditions at the outer surface of the cell. The cell model approach has been shown to have limitations in situations where electrical ion-ion correlations are important (mainly in conditions of

multivalent ions in solution or high particle concentrations), but it may be a reasonable approach for monovalent ions in the solution at moderate particle concentration and surface charge [21,34–36].

Unlike the more rigorous microscopic descriptions, mostly developed for equilibrium conditions, phenomenological or macroscopic models like those based on the cell concept are suited to making predictions for equilibrium and nonequilibrium situations at the cost of overlooking some details that of course might be important, as the above-described individual ion-ion correlations that are neglected in the average approach. These correlations have shown to be crucial in some simulations predicting the charge reversal phenomenon in the presence of multivalent ions, classically out of the scope of cell models. But quite recently, it has been shown that mean field descriptions including finite ion size effects can account for the charge reversal phenomena under appropriate conditions, as high electrolyte concentrations, low particles charge and high counterion valences [37]. This reinforces the use of the cell models as valuable predictors for many electrokinetic and transport phenomena with concentrated colloids, covering electrophoresis in static or alternating electric fields, complex electrical conductivity and dielectric response, sedimentation velocity and potential, electroacoustic response, porous or soft particle electrostatics, effective viscosity or electroviscous effects, etc.

In this work, highly charged spherical colloids in salt-free environments have been chosen, in order to explore in larger detail the phenomenon of counterion condensation, of special relevance in the salt-free limit. The condensation of counterions onto the particle surface plays an outstanding role in general soft-matter, controlling not only its stability but also the self-assembly of bionanomaterials or the compaction of genetic material [38]. The condensation layer is the result of the competition between favorable changes in electrostatic energy as counterions are electrostatically attracted to the highly charged particle and an unfavorable loss of entropy as they are accumulated in a layer close to the particle surface [31,39–42].

The main objective of the present work is the theoretical analysis of the *ac* electrokinetics of salt-free concentrated colloids in realistic aqueous solutions, with inclusion of finite-size effects of chemical species. Consideration of chemical reactions of species in such realistic solutions unavoidably needs of a nonequilibrium kinetic formalism, since chemical equilibrium is not guaranteed under the influence of an *ac* electric field of arbitrarily high frequency. Additionally, we will include finite-size effects in the kinetic equations governing the nonequilibrium scenario for chemical reactions accounting for the association-dissociation processes in aqueous environments. The results will be compared to previous ones assuming pointlike species.

In summary, the present model is intended to be valid for realistic aqueous salt-free colloids of arbitrary particle radius (nanosubmicron range) and particle surface charge, and from dilute to high particle concentrations. Of course, the higher the particle charge density in salt-free solutions, the smaller the particle volume fraction experimentally attainable because of the enhancement of repulsive electrical particle-particle interactions. For the largest surface charge densities available with

typical polymer colloids in laboratories, particle volume fractions of 20% can be reasonably attained. For smaller surface charge densities, larger volume fractions than the latter are easily achieved. In addition, the model is valid for *ac* electric fields of frequency below the GHz range (dielectric relaxation of water molecules is not taken into account) including the zero frequency limit (*dc*). However, the effects of finite size of chemical species on electrokinetic properties should be more noticeable the smaller the particle radius and the larger the particle volume fraction, as the volume available for the ions in solution is greatly reduced.

Careful experiments have to be developed to check the theory. Available electrophoretic techniques in *ac* fields and concentrated colloids are restricted to frequencies below 100 MHz, and are based on electroacoustic effects. For dilute systems, electrophoretic techniques based on laser Doppler velocimetry are developed for *dc* low-strength electric fields. Recent super-heterodyne dynamic light scattering methods are used to measure the *dc* electrophoretic mobility in concentrated systems as well [43]. In the future, appropriate experiments with realistic salt-free colloids have to be carefully designed to test the models. Also, the model might be adequate for aqueous colloids in microfluidic applications, where size effects of chemical species can be a priori important, without using molecular or dynamic simulation techniques, more rigorous than our mean field approach but requiring a huge computational cost, and mainly for equilibrium conditions.

II. FINITE-SIZE EFFECTS AT EQUILIBRIUM

In this section we will explore a scheme for equilibrium mass-action equations before addressing the study of the electrokinetic response of our system in the presence of an alternating electric field. As it was already mentioned in the previous section, use will be made of a spherical cell model (the Kuwabara cell model [44]) to account, in an average sense, for the particle-particle electrohydrodynamic interactions in the colloid. According to this model, the outer radius of the cell, b , will be chosen by equating the particle volume fraction ϕ of the whole colloid with that obtained with a single cell, which is composed of one particle of radius a at its center and a surrounding region of solution of radius b such that $\phi = (a/b)^3$.

We assume for the moment that our system consists of a collection of spherical nanoparticles, with radius a , and surface charge density σ in an aqueous solution with relative permittivity ϵ_{rs} and viscosity η_s , containing n ionic species ($i = 1, 2, \dots, n$) as well as m neutral species ($i = n + 1, \dots, n + m$), with number concentration and activity coefficients n_i^0, γ_i^0 ($i = 1, \dots, N$) [$N = n(\text{ions}) + m(\text{neutral molecules})$], respectively. In the present work equal Bikerman-like equilibrium activity coefficients, γ^0 , for all ionic and neutral species (water molecules excluded) have been chosen and can be expressed as [45]

$$\gamma^0(r) = \frac{1}{1 - \sum_{j=1}^N \frac{n_j^0(r)}{n_j^{\max}}}, \quad (1)$$

with n_j^{\max} ($j = 1, \dots, N = n + m$) as the maximum concentration of j th species due to the excluded volume effect. It must be noted that the Bikerman's approach is the simplest one when dealing with finite-size ions, and that the contribution of Carnahan and Starling [46] provided a much more exact evaluation (the CS model), not suffering of the limitations of Bikerman's. In addition, the method was generalized to solutions containing different types of ions by Boublik [47] and Mansoori *et al.* [48], in what is now known as BM-CSL (Boublik-Mansoori-Carnahan-Starling-Leland) model. The CS model was soon applied to the improvement of Poisson-Boltzmann equation for the description of the EDL (see, e.g., Ref. [49]), and a careful comparison between Bikerman and CS results for the description of the equilibrium double layer, reported by López-García *et al.* [50], demonstrated that the CS model introduces more significant modifications of Poisson-Boltzmann equation for pointlike species than Bikerman model does. The latter only differs from the former when the surface charge density of the particles and/or the ions concentrations in solutions are high. This has been confirmed by Jiménez *et al.* [51] when dealing with highly charged electrodes for use in capacitive energy production. For our purposes, it is more interesting to consider the implications of using one or the other when dealing with the electrokinetic properties of colloids. The calculations carried out by López-García *et al.* [50,52] indicated that the predictions of *dc* electrophoretic mobility according to Bikerman and CS models differ moderately only for electrolyte concentrations above 1 mM (which will be hardly achieved for salt-free systems as it is our case). Furthermore, no data exist regarding the frequency dependence of the dynamic electrophoretic mobility, but it is very significant that the predictions of the dielectric relaxation of the suspensions are almost identical in both models. Considering the computational difficulties involved in the calculation of all frequency dependencies in the case of concentrated, realistic, salt-free systems out of equilibrium, this is a fortunate result, that points to the validity of our conclusions based on the Bikerman model. In the case of pure salt-free systems, only Ohshima [31] has considered the application of CS conditions to the *dc* electrophoretic mobility of such systems.

The equilibrium electrochemical potential for all ions, $\mu_k^0(r)$ ($k = 1, \dots, n$), can be expressed as

$$\mu_k^0(r) = \mu_k^\infty + z_k e \Psi^0(r) + k_B T \ln \left[\frac{n_k^0(r)}{1 - \sum_{j=1}^N \frac{n_j^0(r)}{n_j^{\max}}} \right] \quad (2)$$

and the chemical potential for neutral molecules $\mu_l^0(r)$ ($l = n + 1, \dots, n + m$) as

$$\mu_l^0(r) = \mu_l^\infty + k_B T \ln \left[\frac{n_l^0(r)}{1 - \sum_{j=1}^N \frac{n_j^0(r)}{n_j^{\max}}} \right], \quad (3)$$

where μ_i^∞ and z_i ($i = 1, \dots, N = n + m$) are the electrochemical potential of the i th species at a standard state and its valence (zero for neutral species), respectively. Also, $\Psi^0(r)$ is the equilibrium electric potential at a radial distance r from the center of the particle, e is the elementary electric charge, k_B is the Boltzmann constant and T is the absolute temperature.

In the absence of an external electric field, the Nernst-Planck equations can be solved for the equilibrium concentration of species, as the gradient of their corresponding (electro)chemical potentials must be zero:

$$\nabla \mu_i^0(r) = \nabla \left\{ \mu_i^\infty + z_i e \Psi^0(r) + k_B T \ln [\gamma^0(r) n_i^0(r)] \right\} = 0 \quad (i = 1, \dots, n + m = N). \quad (4)$$

Contrary to the case of low particle volume fraction, the bulk values of the concentrations of ions and neutral species are not well defined when the particle volume fraction is high, due to possible overlapping of electric double layers of adjacent particles. A reasonable approximation to the equilibrium bulk concentration of chemical species might be its value on the outer surface of the cell $r = b$, where the equilibrium electric potential $\Psi^0(b)$ is set to zero.

Thus, we obtain for ionic species,

$$n_i^0(r) = \left[\frac{1 - \sum_{j=1}^N \frac{n_j^0(r)}{n_j^{\max}}}{1 - \sum_{j=1}^N \frac{b_j}{n_j^{\max}}} \right] b_i e^{-\frac{z_i e}{k_B T} \Psi^0(r)} \quad (i = 1, \dots, n), \quad (5)$$

and for neutral molecules,

$$n_i^0(r) = \left[\frac{1 - \sum_{j=1}^N \frac{n_j^0(r)}{n_j^{\max}}}{1 - \sum_{j=1}^N \frac{b_j}{n_j^{\max}}} \right] b_i \quad (i = n + 1, \dots, n + m), \quad (6)$$

where the b_i ($i = 1, \dots, n + m = N$) coefficients are the corresponding ion or neutral molecule concentrations at the outer surface of the cell, $r = b$. By summing over all species, the term between brackets in Eqs. (5) and (6) can be obtained. Therefore, for ions we have

$$n_i^0(r) = \frac{b_i e^{-\frac{z_i e}{k_B T} \Psi^0(r)}}{1 + \sum_{j=1}^n \frac{b_j}{n_j^{\max}} [e^{-\frac{z_j e}{k_B T} \Psi^0(r)} - 1]} \quad (i = 1, \dots, n), \quad (7)$$

and for neutral species,

$$n_i^0(r) = \frac{b_i}{1 + \sum_{j=1}^n \frac{b_j}{n_j^{\max}} [e^{-\frac{z_j e}{k_B T} \Psi^0(r)} - 1]} \quad (i = n + 1, \dots, n + m). \quad (8)$$

The modified Poisson-Boltzmann equation (MPB) accounting for the finite size of the ions is then

$$\nabla^2 \Psi^0(r) = -\frac{e}{\epsilon_0 \epsilon_{rs}} \frac{\sum_{i=1}^n z_i b_i e^{-\frac{z_i e}{k_B T} \Psi^0(r)}}{1 + \sum_{j=1}^n \frac{b_j}{n_j^{\max}} [e^{-\frac{z_j e}{k_B T} \Psi^0(r)} - 1]}. \quad (9)$$

Borukhov *et al.* [53] obtained a similar modified Poisson-Boltzmann equation (MPB) accounting for the excluded volume effect of ions in solution around a spherical particle by the functional derivatives of the total free energy with respect to the equilibrium electric potential and the ionic concentrations. Following Borukhov's method, an alternative derivation of the latter equations for the simple case where all ions and neutral molecules different than those of the solvent have the same size (or equivalently, equal maximum concentration n^{\max} due to the excluded volume effect) is shown in Sec. S1 of the Supplementary Information File (SIF) [54]. The same free-energy procedure was already used for the analysis of the

equilibrium double layer of a realistic salt-free colloid with a classical equilibrium formalism for chemical reactions in solution [55].

The Nernst-Planck equations for ions and neutral molecules different than water lead to the following results:

$$\left[\frac{\gamma^0(b)}{\gamma^0(r)} \right] = \frac{1}{1 + \sum_{j=1}^n \frac{b_j}{n_j^{\max}} [e^{-\frac{z_j e}{k_B T} \Psi^0(r)} - 1]}, \quad (10)$$

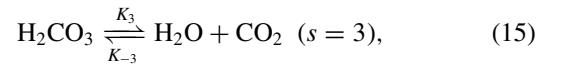
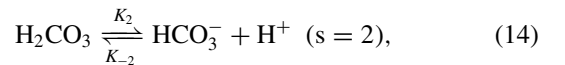
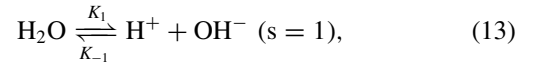
$$n_i^0(r) \gamma^0(r) = \gamma^0(b) b_i e^{-\frac{z_i e}{k_B T} \Psi^0(r)} \quad (i = 1, \dots, n), \quad (11)$$

$$n_i^0(r) \gamma^0(r) = \gamma^0(b) b_i \quad (i = n + 1, \dots, n + m), \quad (12)$$

where, as it was already described, a common activity coefficient $\gamma^0(r)$ has been assumed for all the species.

A common situation for aqueous colloids is that of having hydronium or hydroxyl ions as added counterions in solution. This is so because the use of ion-exchange resins in laboratories typically substitutes the original added counterions released by the particles by one of the latter two, depending on the sign of the counterion. In the present case, the ionic species acting finally as the added one will be H^+ , and may have different contributions: one part equivalent to the released countercharge and another one stemming from the water dissociation coupled to the chemical reactions of the carbonic acid generation and dissociation in solution.

The reactions are



where K_s , K_{-s} are the forward and reverse rate constants [56,57]. For these equations, $K_{-1} = 1.11 \times 10^{11}$ L/(mol.s), $K_{-2} = 5.0 \times 10^{10}$ L/(mol.s) and $K_{-3} = 7.03 \times 10^{-4}$ L/(mol.s). The other kinetic constants can be found from the equilibrium constants for each reaction: $(K_1/K_{-1}) c_{H_2O}^0 = 10^{-14}$ mol²/L², $K_2/K_{-2} = 2.5 \times 10^{-14}$ mol/L, $(K_{-3}/K_3) c_{H_2O}^0 = 1.7 \times 10^{-3}$, with $c_{H_2O}^0 = 55.5$ mol/L as the molar concentration of water. As we are assuming that free water acts as an ideal solvent, its activity coefficient is assumed to be $\gamma_{H_2O} = 1$, and will not appear in any of the corresponding mass-action equations of the latter opposite elementary chemical reactions [58]. As mentioned, the equilibrium mass-action equations are assumed to be fulfilled locally everywhere in the solution, and not just in the bulk. By using Eqs. (11) and (12), we can write

$$\begin{aligned} \frac{K_1}{K_{-1}} &= \frac{n_{H^+}^0(r) \gamma_{H^+}^0(r) n_{OH^-}^0(r) \gamma_{OH^-}^0(r)}{n_{H_2O}^0} \\ &= \frac{n_{H^+}^0(r) n_{OH^-}^0(r) [\gamma^0(r)]^2}{n_{H_2O}^0} = \frac{b_{H^+} b_{OH^-}}{b_{H_2O}} [\gamma^0(b)]^2, \end{aligned} \quad (16)$$

$$\frac{K_2}{K_{-2}} = \frac{n_{HCO_3^-}^0(r) \gamma_{HCO_3^-}^0(r) n_{H^+}^0(r) \gamma_{H^+}^0(r)}{n_{H_2CO_3}^0(r) \gamma_{H_2CO_3}^0(r)}$$

$$= \frac{n_{\text{HCO}_3^-}^0(r) n_{\text{H}^+}^0(r) [\gamma^0(r)]}{n_{\text{H}_2\text{CO}_3}^0(r)} = \frac{b_{\text{HCO}_3^-} b_{\text{H}^+}}{b_{\text{H}_2\text{CO}_3}} [\gamma^0(b)], \quad (17)$$

$$\begin{aligned} \frac{K_3}{K_{-3}} &= \frac{n_{\text{CO}_2}^0(r) \gamma_{\text{CO}_2}^0(r) n_{\text{H}_2\text{O}}^0}{n_{\text{H}_2\text{CO}_3}^0(r) \gamma_{\text{H}_2\text{CO}_3}^0(r)} \\ &= \frac{n_{\text{CO}_2}^0(r) n_{\text{H}_2\text{O}}^0}{n_{\text{H}_2\text{CO}_3}^0(r)} = \frac{b_{\text{CO}_2} b_{\text{H}_2\text{O}}}{b_{\text{H}_2\text{CO}_3}}, \end{aligned} \quad (18)$$

where $b_{\text{H}_2\text{O}} = n_{\text{H}_2\text{O}}^0 = 10^3 N_A c_{\text{H}_2\text{O}}^0$ and N_A is Avogadro's number. In the situation considered, we will have three ionic species in solution, namely, H^+ , OH^- , and HCO_3^- , and two neutral species, dissolved CO_2 in equilibrium with the standard atmosphere, and H_2CO_3 . The modified Poisson-Boltzmann equation (MPB) [Eq. (9)] in conjunction with Eqs. (16)–(18), can be solved by the iterative procedure described in Sec. 2 of the SIF.

III. ELECTROKINETIC EQUATIONS AND BOUNDARY CONDITIONS IN *ac* FIELDS

A. Electrokinetic equations

Let us now consider a spherical particle of radius a , surface charge density σ , mass density ρ_p and relative permittivity ε_{rp} surrounded by a shell of the above described realistic aqueous solution of outer radius $b = a \phi^{-1/3}$. An alternating electric field $\vec{E} \exp(-i\omega t)$ of angular frequency ω is applied to the system. In the stationary state, the particle will move with a velocity $\vec{V}_p \exp(-i\omega t)$ where $\vec{V}_p = \mu \vec{E}$, with μ as the dynamic electrophoretic mobility. A spherical coordinate system (r, θ, φ) is fixed at the center of the particle, and the polar axis ($\theta = 0$) is chosen to be parallel to the applied electric field.

The fundamental equations connecting the electrical potential $\Psi(\vec{r}, t)$, the number density of each species $n_i(\vec{r}, t)$ and their drift velocity $\vec{v}_i(\vec{r}, t)$ ($i = 1, \dots, n + m$), the fluid velocity $\vec{v}(\vec{r}, t)$ and the pressure $P(\vec{r}, t)$ at every point \vec{r} in the system and time t are

$$\nabla^2 \Psi(\vec{r}, t) = -\frac{\rho_{el}(\vec{r}, t)}{\varepsilon_{rs} \varepsilon_0}, \quad (19)$$

$$\rho_{el}(\vec{r}, t) = \sum_{i=1}^n z_i e n_i(\vec{r}, t), \quad (20)$$

$$\eta_s \nabla^2 \vec{v}(\vec{r}, t) - \nabla P(\vec{r}, t) - \rho_{el}(\vec{r}, t) \nabla \Psi(\vec{r}, t) = \rho_s \frac{\partial}{\partial t} [\vec{v}(\vec{r}, t) + \vec{V}_p \exp(-i\omega t)], \quad (21)$$

$$\nabla \cdot \vec{v}(\vec{r}, t) = 0, \quad (22)$$

$$\vec{v}_i(\vec{r}, t) = \vec{v}(\vec{r}, t) - \frac{1}{\lambda_i} \nabla \mu_i(\vec{r}, t) \quad (i = 1, \dots, n + m), \quad (23)$$

$$\mu_i(\vec{r}, t) = \mu_i^\infty + z_i e \Psi(\vec{r}, t) + k_B T \ln[\gamma_i(\vec{r}, t) n_i(\vec{r}, t)] \quad (i = 1, \dots, n + m), \quad (24)$$

$$\nabla \cdot [n_i(\vec{r}, t) \vec{v}_i(\vec{r}, t)] = \Xi_i(\vec{r}, t) - \frac{\partial n_i(\vec{r}, t)}{\partial t} \quad (i = 1, \dots, n + m). \quad (25)$$

Equation (19) is Poisson's equation, where $\rho_{el}(\vec{r}, t)$ is the electric charge density [Eq. (20)] and ε_0 the vacuum permittivity. Equations (21) and (22) are the Navier-Stokes equations for an incompressible fluid flow of viscosity η_s and mass density ρ_s at low Reynolds number in the presence of an electrical body force. Equation (23) derives from the Nernst-Planck equation for the flow of the i th species, including the gradient of its (electro)chemical potential $\mu_i(\vec{r}, t)$ defined in Eq. (24), where again μ_i^∞ is its standard value and λ_i its drag coefficient. Equation (25) is the continuity equation for the conservation of each species including the possibility of generation and annihilation of species by chemical reactions where $\Xi_i(\vec{r}, t)$ are generation-recombination functions for the ions and neutral molecules.

In the case we are concerned, $n = 3$ and $m = 2$, that, as mentioned, correspond to: ions H^+ ($i = 1$) from dissociation of ionizable particle surface groups, water dissociation and dissociation of carbonic acid generated by atmospheric CO_2 dissolved in the solution, OH^- ($i = 2$) from water dissociation, and bicarbonate ion HCO_3^- ($i = 3$) and the neutral species H_2CO_3 ($i = 4$, $z_4 = 0$) and CO_2 ($i = 5$, $z_5 = 0$) from the atmospheric contamination.

For the ions, the functions $\Xi_i(\vec{r}, t)$ ($i = 1, \dots, 3$) are expressed as

$$\begin{aligned} \Xi_1(\vec{r}, t) = \Xi_{\text{H}^+}(\vec{r}, t) &= [K_1 n_{\text{H}_2\text{O}}^0 - K_{-1} n_{\text{H}^+}(\vec{r}, t) n_{\text{OH}^-}(\vec{r}, t) \gamma_{\text{H}^+}(\vec{r}, t) \gamma_{\text{OH}^-}(\vec{r}, t)] + [K_2 n_{\text{H}_2\text{CO}_3}(\vec{r}, t) \gamma_{\text{H}_2\text{CO}_3}(\vec{r}, t) \\ &\quad - K_{-2} n_{\text{HCO}_3^-}(\vec{r}, t) n_{\text{H}^+}(\vec{r}, t) \gamma_{\text{HCO}_3^-}(\vec{r}, t) \gamma_{\text{H}^+}(\vec{r}, t)], \end{aligned} \quad (26)$$

$$\Xi_2(\vec{r}, t) = \Xi_{\text{OH}^-}(\vec{r}, t) = [K_1 n_{\text{H}_2\text{O}}^0 - K_{-1} n_{\text{H}^+}(\vec{r}, t) n_{\text{OH}^-}(\vec{r}, t) \gamma_{\text{H}^+}(\vec{r}, t) \gamma_{\text{OH}^-}(\vec{r}, t)], \quad (27)$$

$$\Xi_3(\vec{r}, t) = \Xi_{\text{HCO}_3^-}(\vec{r}, t) = [K_2 n_{\text{H}_2\text{CO}_3}(\vec{r}, t) \gamma_{\text{H}_2\text{CO}_3}(\vec{r}, t) - K_{-2} n_{\text{HCO}_3^-}(\vec{r}, t) n_{\text{H}^+}(\vec{r}, t) \gamma_{\text{HCO}_3^-}(\vec{r}, t) \gamma_{\text{H}^+}(\vec{r}, t)]. \quad (28)$$

In addition, for the neutral species ($i = 4, 5$) we have

$$\begin{aligned} \Xi_4(\vec{r}, t) = \Xi_{\text{H}_2\text{CO}_3}(\vec{r}, t) = & -[K_2 n_{\text{H}_2\text{CO}_3}(\vec{r}, t) \gamma_{\text{H}_2\text{CO}_3}(\vec{r}, t) - K_{-2} n_{\text{HCO}_3^-}(\vec{r}, t) n_{\text{H}^+}(\vec{r}, t) \gamma_{\text{HCO}_3^-}(\vec{r}, t) \gamma_{\text{H}^+}(\vec{r}, t)] \\ & - [K_3 n_{\text{H}_2\text{CO}_3}(\vec{r}, t) \gamma_{\text{H}_2\text{CO}_3}(\vec{r}, t) - K_{-3} n_{\text{H}_2\text{O}}^0 n_{\text{CO}_2}(\vec{r}, t) \gamma_{\text{CO}_2}(\vec{r}, t)], \end{aligned} \quad (29)$$

$$\Xi_5(\vec{r}, t) = \Xi_{\text{CO}_2}(\vec{r}, t) = [K_3 n_{\text{H}_2\text{CO}_3}(\vec{r}, t) \gamma_{\text{H}_2\text{CO}_3}(\vec{r}, t) - K_{-3} n_{\text{H}_2\text{O}}^0 n_{\text{CO}_2}(\vec{r}, t) \gamma_{\text{CO}_2}(\vec{r}, t)], \quad (30)$$

according to the procedure developed by Baygents and Saville for weak electrolytes [59]. In Sec. 3 of the SIF the linear perturbation scheme, that has been applied to solve the latter set of electrokinetic differential equations in the presence of low-strength alternating electric fields, is studied in detail. Also, the symmetry of the problem has facilitated the mathematical tasks concerning the field-induced linear perturbations in our spherical colloid.

B. Boundary conditions

The appropriate boundary conditions are [60]

$$\Psi_p(\vec{r}) = \Psi(\vec{r}) \text{ at } r = a, \quad (31)$$

$$\varepsilon_{rs} \nabla \Psi(\vec{r}, t) \cdot \hat{r} - \varepsilon_{rp} \nabla \Psi_p(\vec{r}, t) \cdot \hat{r} = -\sigma/\varepsilon_0 \text{ at } r = a, \quad (32)$$

$$\vec{v}(\vec{r}) = 0 \text{ at } r = a, \quad (33)$$

$$\vec{v}_j(\vec{r}) \cdot \hat{r} = 0 \quad (j = 1, \dots, 5) \text{ at } r = a, \quad (34)$$

$$\langle \rho_m \vec{u}' \rangle = \frac{1}{V_{\text{cell}}} \int_{V_{\text{cell}}} \rho_m \vec{u}' dV = 0, \quad (35)$$

$$\vec{\omega}(\vec{r}) = \nabla \times \vec{v}(\vec{r}) = 0 \text{ at } r = b, \quad (36)$$

$$\delta n_j(\vec{r}) = 0 \quad (j = 1, \dots, 5) \text{ at } r = b, \quad (37)$$

$$\delta \Psi(\vec{r}) = -\vec{E} \cdot \vec{r} \text{ at } r = b, \quad (38)$$

where ρ_m is the local mass density, and \vec{u}' is the local velocity with respect to a laboratory reference system.

At the particle surface, some boundary conditions have to be imposed: the continuity of the electric potential, as expressed by Eq. (31); Eq. (32) represents the discontinuity of the normal component of the displacement vector (\hat{r} is the radial unit vector of the spherical coordinate system); Eq. (33) indicates that the fluid is at rest at the particle surface in the reference system fixed to the particle; Eq. (34) stands for the impossibility of ions to penetrate the solid particle; according to O'Brien [61] the condition of zero macroscopic momentum per unit volume of the colloid [see Eq. (35)] must be fulfilled, allowing us to obtain the dynamic electrophoretic mobility. At the outer surface of the cell we have Eq. (36), which stands for the Kuwabara boundary condition of null vorticity for the fluid velocity, and Eqs. (37) and (38), which are the Shilov-Zharkikh-Borkovskaya boundary conditions [17] for the perturbed concentration of species and perturbed electric potential in such surface. Finally, the equation of motion of the unit cell with the net force acting on it (see Sec. S6 of SIF) will permit us to close the problem.

In Sec. 3 of the SIF the linearized version of the latter boundary conditions can be found, according to the

above-mentioned linear perturbation scheme for low-strength alternating electric fields we are concerned in this work. In addition, in Sec. S4 of the SIF the condition of zero macroscopic momentum per unit volume of the colloid shown in Eq. (35) is studied in detail. Furthermore, the perturbation pressure function is derived by integration of the Navier-Stokes equation in Sec. S5 of the SIF, and the net force acting on the unit cell is addressed in Sec. S6 of the SIF.

As the complex relative permittivity ε_r^* of the system does help in properly understanding the frequency dependence of the particle dynamic mobility μ , its determination becomes very convenient. Usually, ε_r^* is directly obtained from the complex conductivity K^* of the suspension, which is evaluated by the linear relation connecting macroscopic electric current density, $\langle \vec{i}(\vec{r}, t) \rangle$, and macroscopic electric field in the cell, $\langle -\nabla \Psi(\vec{r}, t) \rangle$. The macroscopic quantities stand for volume averages of the corresponding local quantities in the volume of a cell. Thus, in Sec. S7 of the SIF the complex relative permittivity of the colloid will be derived from its complex electrical conductivity. Finally, in Sec. S8 of the SIF, and for convenience for the numerical resolution of the electrokinetic equations set, the dimensionless form of linearized electrokinetic equations and boundary conditions can be found.

IV. RESULTS AND DISCUSSION

A. Finite-size effects: Overall behavior

Figure 1 gives us information about the concentration profiles predicted by the model for two sizes of chemical species. If a simple cubic packing (52.35% occupancy) is considered, and an equal value n^{max} is chosen for the maximum concentration of neutral and charged species, then we have $n^{\text{max}} = (2R)^{-3}$, with $2R$ as the diameter of the chemical species, $n^{\text{max}} = 10^3 N_A c^{\text{max}}$, with c^{max} the maximum molar concentration of species. When $c^{\text{max}} = 4.0$ mol/L, we have an effective diameter $2R = 0.75$ nm, and when $c^{\text{max}} = 2.5$ mol/L, the effective diameter is 0.87 nm, both in the typical range of hydrated ions [62]. In all the cases analyzed, the ‘‘added counterions’’ have been H^+ .

The equilibrium molar concentration of H^+ is displayed in Fig. 1(a), according to the present model [RS model (realistic with finite-size effects) hereafter] in a region very close to the particle surface. The two sizes mentioned for chemical species are included for comparison as well as the realistic pointlike prediction (RP model hereafter), which is attained from the full model when the maximum concentration of species n^{max} tends to infinity (the pointlike limit). Analogously, in Fig. 1(b) we show similar predictions of the equilibrium concentrations of neutral molecules and coions in the solution for the same cases studied. As it has been reported in the literature [63,64],

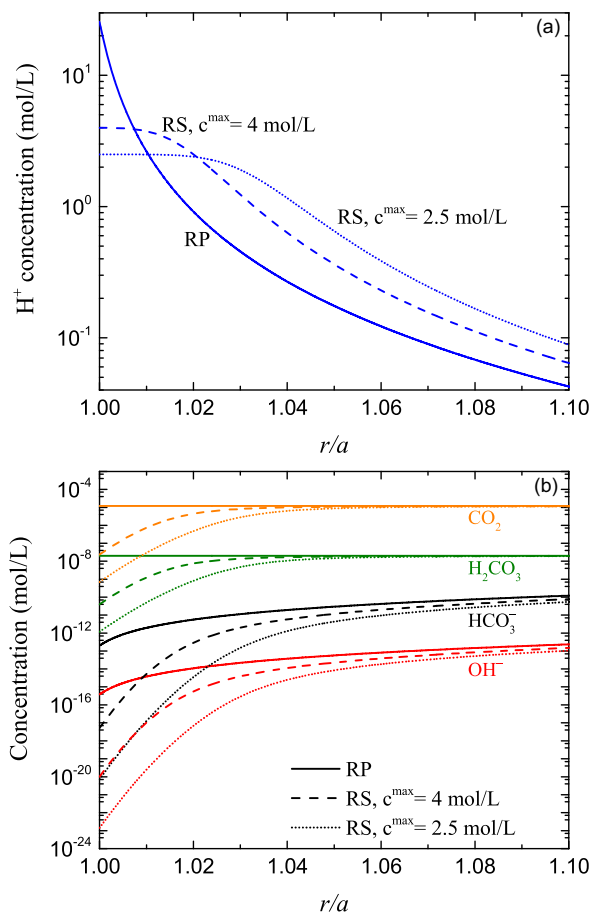


FIG. 1. (a) Equilibrium molar concentration of added counterions H^+ as a function of the dimensionless radial distance $x = r/a$ from the particle center inside the cell. (b) Equilibrium molar concentrations of neutral molecules and coions as a function of x . From top to bottom: CO_2 , H_2CO_3 , HCO_3^- , OH^- . Solid lines: realistic salt-free pointlike predictions (model RP); dashed ($c^{\max} = 4.0$ mol/L) and dotted ($c^{\max} = 2.5$ mol/L) lines: realistic, salt-free, finite-size (RS) predictions. Data: $\phi = 0.0001$, $a = 25$ nm, $\sigma = -30.0 \mu C/cm^2$, $x = b/a = 21.54$.

when the species are allowed to have finite size, the maximum concentration of counterions can give rise to a concentration plateau very close to the particle surface for sufficiently high particle charges, like the one displayed in Fig. 1(a). Instead, for the PB approach the pointlike counterion concentration monotonously increases as we get closer to the particle surface from the solution, reaching unrealistic values in many situations with highly charged particles. Also, as ion size increases, the maximum concentration of species diminishes close to the particle surface and the width of the concentration plateau increases. It is also remarkable that the equilibrium concentrations of coions and neutral molecules in Fig. 1(b) are lower than the RP predictions, the more so the larger the size of the species, although the pointlike results are practically recovered just a few nanometers from the particle surface ($x = 1.0$ means $r = a = 25$ nm, $x = 1.1$ means $r = 27.5$ nm, and $x = b/a = 21.54$ corresponds to $r = b = 538.5$ nm, the outer radius of the cell).

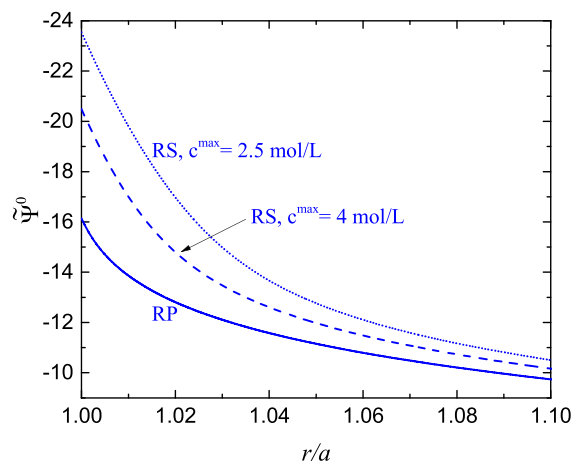


FIG. 2. Dimensionless equilibrium electric potential as a function of dimensionless radial distance $x = r/a$ from the particle center inside the cell, for the models and conditions indicated in Fig. 1. Data: $\phi = 0.0001$, $a = 25$ nm, $\sigma = -30.0 \mu C/cm^2$, $x = b/a = 21.54$.

In Fig. 2, the dimensionless equilibrium electrical potential $\Psi^0 = e\psi^0/k_B T$ is displayed as a function of the dimensionless radial distance r/a close to the particle surface, for the same realistic pointlike and full finite-size conditions studied in Fig. 1. The most important feature than can be drawn from Fig. 2 is the increase of the electrical potential at every distance from the particle surface when the chemical species are allowed to have finite size. In other words, the larger size of species leads to a decrease of the population of counterions close to the charged surface, and therefore, to a decrease of the screening of particle charge. As it will be shown later, this fact will have important consequences on the high frequency electrophoretic mobility.

Figure 3 illustrates the real (a) and imaginary (b) parts of the dimensionless dynamic electrophoretic mobility $\tilde{\mu} = 3\eta_s e / (2\epsilon_{rs} \epsilon_0 k_B T) \mu$, as a function of the frequency of the alternating electric field for realistic pointlike and realistic finite-size (full model) predictions, and for the two finite sizes of species studied in previous figures. The first feature worth to consider in the frequency dependence of $\text{Re}(\tilde{\mu})$ is its increase around 10^6 Hz: this is a manifestation of the Maxwell-Wagner-O'Konski (MWO) relaxation [65,66]. This is the phenomenon by which the induced dipole associated to ionic rearrangements in the EDL due to the electric field, cannot be built up because the frequency of the field is too high for such rearrangements to occur: the induced dipole associated to the ionic rearrangements in the EDL produces a braking of the particle motion that relaxes for the frequency range mentioned. This relaxation corresponds to the lowest-frequency minimum of the imaginary part of the mobility in Fig. 3(b). The subsequent diminution of $\tilde{\mu}$ in Fig. 3(a) as frequency increases after the first mobility maximum is related to the inertia of particle and fluid, but there is another relaxation process at larger frequencies (around 10^9 Hz). This can be interpreted as an additional Maxwell-Wagner process, similar to the MWO above discussed, but associated in this case to the rearrangement of the thin layer of counterions (condensate), that develops close to the particle surface in highly charged

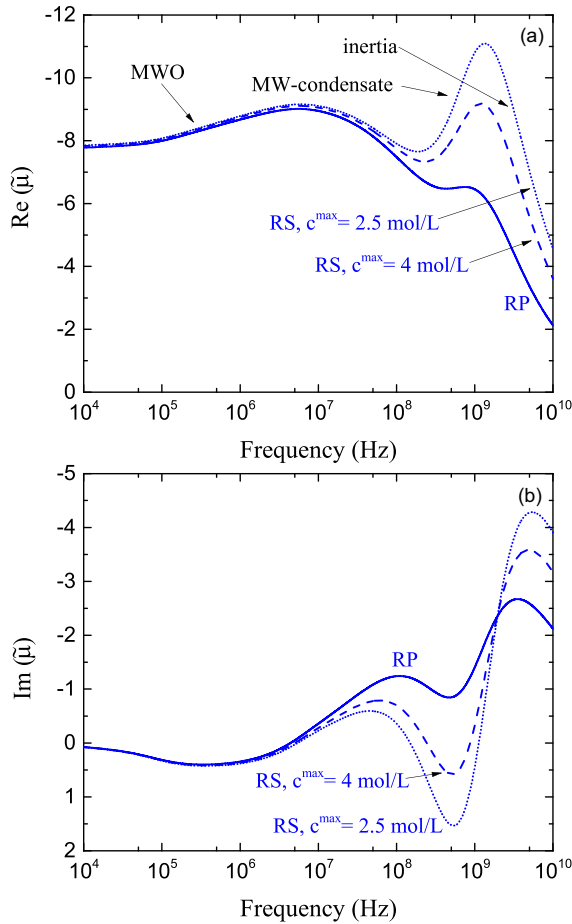


FIG. 3. Real (a) and imaginary (b) parts of the dimensionless dynamic electrophoretic mobility $\tilde{\mu}$ as a function of the frequency of the alternating electric field. Solid lines: realistic salt-free pointlike predictions (model RP); dashed ($c^{\max} = 4.0$ mol/L) and dotted ($c^{\max} = 2.5$ mol/L) lines (full model or model RS): realistic salt-free finite-size predictions, for the indicated maximum concentrations. Data: $\phi = 0.0001$, $a = 25$ nm, $\sigma = -30.0$ $\mu\text{C}/\text{cm}^2$.

colloids [31]. Similarly to the freezing of the MWO relaxation above mentioned, the reordering of the condensate also ceases above a characteristic frequency, which is above the MWO relaxation because of the small thickness of the condensate. The imaginary part of the dynamic mobility in Fig. 3(b) helps us again to better identify the relaxation frequency of this second MW-process, as it coincides with that of the highest-frequency minimum (around 6×10^8 Hz in this representation). As it is clearly shown in Fig. 3, in the low frequency region, both realistic pointlike and full model finite-size predictions show essentially no differences whatever the finite size chosen. This situation is basically due to the fact that it is the diffuse layer response which mainly governs the mobility in such frequency region. The low-frequency induced electric dipole moment and related relaxation mechanisms hardly change regardless of whether the species are allowed to have finite size or not, due to the typically huge dimensions of double layers in salt-free colloids and the low particle concentration of the colloids chosen in Fig. 3.

Figure 3 also indicates that the RS model predicts an important enhancement of the mobility at the high side of the frequency range, where the MW relaxation of the condensate takes place [31]. The large value of the full dynamic mobility as compared to the pointlike approximation is linked to the larger thickness of the condensate for finite ions. This leads to an important reduction of the screening of the particle surface charge (see also the remarkable increase of the equilibrium electric potential in Fig. 2 as the size of species increases), and to a corresponding enhanced contribution to the electric dipole moment of the condensate region. Its disappearance by MW relaxation gives rise to a huge mobility increase, clearly overcoming the inertial fall. That increase is, as expected, larger the bigger the counterions size.

B. Dynamic electrophoretic mobility and limits of the model

In this section, a more detailed study is proposed with the addition of two limiting predictions which are simplifications of the full model when the realistic chemistry of the aqueous solution is neglected but the species are still allowed to have finite size (NRS model: nonrealistic and finite-size effects, hereafter) and when the species are pointlike and no realistic chemistry is allowed (NRP model: nonrealistic and pointlike, hereafter). The latter two model variations are essentially pure salt-free theoretical limits and differ just in the consideration of whether the added counterions (the only species present) have finite size or not. In summary, the model variations (the reference is the full model developed in this work, or RS model) that will help us with the discussion are:

—RP model. Chemical reactions are taken into account and all the species are pointlike.

—NRS model. Chemical reactions are neglected, and the only source of counterions is that linked to the ionization of chemical surface groups on the particles surface. The counterion species is allowed to have finite size. This prediction should tend to that for pure salt-free colloids with finite counterion size [28]. We attain this limit when chemical reactions in the full model are eliminated, and the electroneutrality preserved with just charged particles and their added counterions as the only countercharge.

—NRP model. Same as NRS model but neglecting the size of counterions. This prediction should tend to that for a pure salt-free colloid with pointlike added counterions [23]. It is attained from the NRS model when the parameter n^{\max} tends to infinity.

To accomplish a first comparison between predictions according to the new model and those of the latter model variations, a representative case will be studied on which general conclusions will be drawn. In Fig. 4 we show for simplicity the analysis of just the real part of the dimensionless dynamic electrophoretic mobility versus the frequency of the alternating electric field. It is interesting to note that the low frequency limit of our calculations for the simplest NRP case, is very close to the derivation carried out by Ohshima [67] for the case of highly charged particles and low volume fractions. This can be taken as an indication of the validity of our general model. A comparison with experimental data obtained in salt-free conditions for the dc electrophoretic mobility of latex particles by Medebach and Palberg [68] was

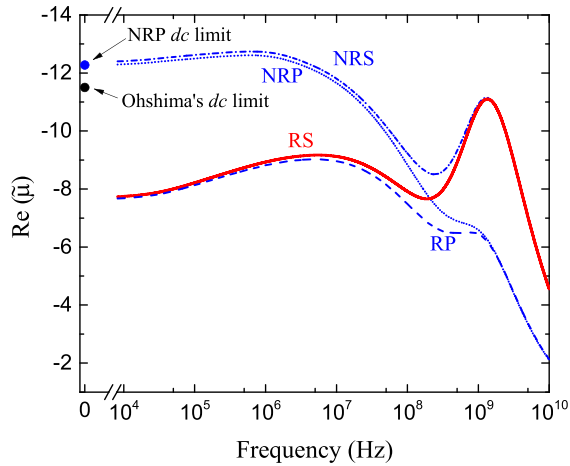


FIG. 4. Real part of the dimensionless dynamic electrophoretic mobility $\tilde{\mu}$ as a function of frequency of the electric field, for the models described (see text). Data: $\phi = 0.00001$, $a = 25$ nm, $c^{\max} = 2.5$ mol/L, $\sigma = -30.0$ $\mu\text{C}/\text{cm}^2$. The dc limits of our model and of Ohshima's high surface charge approximation [67] are indicated for comparison.

carried out by the authors [20], and it was found a reasonable agreement between data and predictions using the RP version of the general model. Additionally, it should be mentioned that Lobaskin *et al.* [69] used molecular dynamics for the simulation of the electrophoretic mobility of the same particles, and found a good agreement with experiments, similarly to the accordance of our model and that set of data.

One of the most remarkable features that can be immediately drawn from Fig. 4 is the huge difference between the low-frequency predictions of pure salt-free and realistic salt-free mobility models. This enormous discrepancy is maintained when finite-size effects are included. In the recent literature, similar differences between realistic and pure salt-free pointlike predictions have been reported [20]. In this work, it is also confirmed that finite size effects have no significant influence on the mobility for both pure (compare NRP and NRS curves) and realistic (compare RP and RS curves) approaches at low to intermediate frequencies for low particle concentrations.

Another striking characteristic observed in Fig. 4 is that at high frequencies, where the MW-process of the condensate region relaxes, the prediction of the NRS model tends to match that of the full realistic model, RS, whereas the pointlike approach, RP, reproduces the full RS results at low or medium frequencies in the dilute particle concentration limit. The overall mobility response [see also Fig. 3(a)] was analyzed above in terms of EDL polarization and MW relaxations, but the coincidence between NRS and RS models at high frequencies suggests that the key factor in determining the frequency response of the mobility is not the realistic consideration of chemical reactions but rather the proper inclusion of size effects. Note that the change of the mobility with frequency in the high-frequency range is mostly related to the MW relaxation of the condensate, populated by counterions, no matter the kind of description of the ionic composition

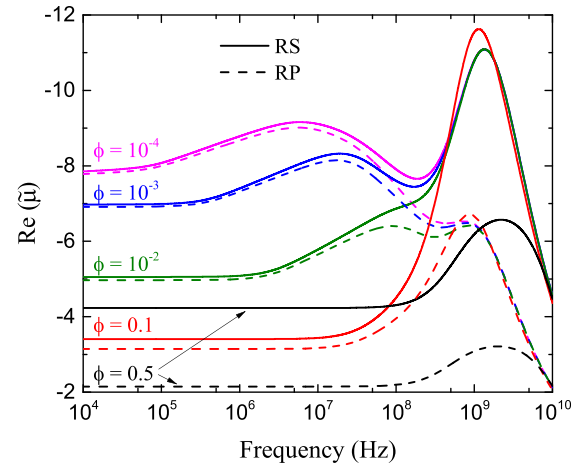


FIG. 5. Real part of the dimensionless dynamic electrophoretic mobility $\tilde{\mu}$ as a function of the frequency of the alternating electric field for the indicated volume fractions and RS model (solid lines) or RP model (dashed lines) predictions. Other data: $c^{\max} = 2.5$ mol/L, $a = 25$ nm, $\sigma = -30.0$ $\mu\text{C}/\text{cm}^2$.

of the EDL. Similar results have been reported for the ideal salt-free description [28].

All these features point to the conclusion that for low concentrated colloids the realistic conditions are crucial at low frequencies, but at very high ones it is the counterion species that plays the most important role, as realistic and pure salt-free results tend to converge regardless of whether the counterions are considered with finite size or pointlike. For this reason, it should be very convenient to study the cases where the role of the counterions increases in importance. This situation is principally attained as particle volume fraction increases, due to the associated enhancement of the population of counterions, and even more if in addition the particles are highly charged. We will address these cases in the following sections.

C. Finite-size effects and particle volume fraction

In Fig. 5 we explore the effect of volume fraction on the real part of the dynamic electrophoretic mobility for a highly charged colloid with the other conditions as in Fig. 4. Note, first of all, that as particle concentration increases, the amount of counterions in solution increases as well. This brings about a shortening of the average interparticle distance and an enhancement of the crowding of counterions in a region close to the particle surface. To this we must add the enhanced particle-particle hydrodynamic interactions, also contributing to an overall reduction of the mobility. However, the high-frequency real part of the dimensionless dynamic mobility increases from roughly 6.5 to 11.5 when the ion size is accounted for at low-moderate volume fractions. Note as well that for moderate to high volume fractions, the low frequency mobility is significantly larger when size effects are taken into account. This is a consequence of the reduced screening of the particle charge due to the limited volume accessible to the finite counterions as compared to pointlike ones in the latter conditions. It is also observed that the diffuse layer MWO process is shifted to the high-frequency side due to the

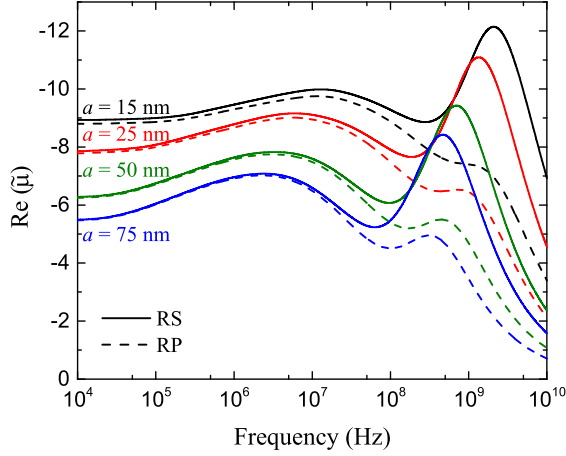


FIG. 6. Same as Fig. 5, but for varying particle radius (indicated in nm), for $\phi = 10^{-4}$ and the rest of parameters unchanged.

increase of the electrical conductivity of the medium by the enhancement of released counterions upon increasing particle volume fraction. As a result, a single, merged MW relaxation band is observed at high volume fractions.

D. The role of particle radius

In Fig. 6 we explore the relative influence of realistic finite-size effects on the real part of the electrophoretic mobility as a function of the frequency of the alternating electric field upon changing particle radius at a given particle volume fraction $\phi = 0.0001$, surface charge density $\sigma = -30.0 \mu\text{C}/\text{cm}^2$, and maximum concentration of species $c^{\text{max}} = 2.5 \text{ mol/L}$ (effective diameter $2R = 0.87 \text{ nm}$). The particle radii chosen are 15, 25, 50, and 75 nm. The data presented show that the main aspects of the $\tilde{\mu}$ -frequency plots are consistently reproduced for all the tested radii, namely, increased importance of the condensate for finite-size ions, and negligible difference in dilute conditions between the RP and RS models at low frequencies. It is worthwhile to mention that as the particle radius increases, the low frequency mobility decreases. This is a well-known classical result [70] for the mobility- κa (κ^{-1} , the Debye length, is representative of the EDL thickness) relationship at the low κa range (<5), as in the case of data in Fig. 6. For the present study, we have estimated κa in terms of the values of the ion concentrations at the outer surface of the cell: b_{H^+} , b_{OH^-} and $b_{\text{HCO}_3^-}$, as

$$\kappa a = \left[\frac{e^2 a^2}{\epsilon_{rs} \epsilon_0 k_B T} (b_{\text{H}^+} z_{\text{H}^+}^2 + b_{\text{OH}^-} z_{\text{OH}^-}^2 + b_{\text{HCO}_3^-} z_{\text{HCO}_3^-}^2) \right]^{1/2}. \quad (39)$$

The κa values estimated are: 0.08, 0.12, 0.25, 0.37, for 15, 25, 50, and 75 nm, respectively. This means that we are in the κa range for which increasing κa leads to a decreasing mobility. This is because the viscous friction increases with size, whereas the effective particle charge is little affected by particle size as most added counterions are located in the condensate, practically compensating for the increase of charge

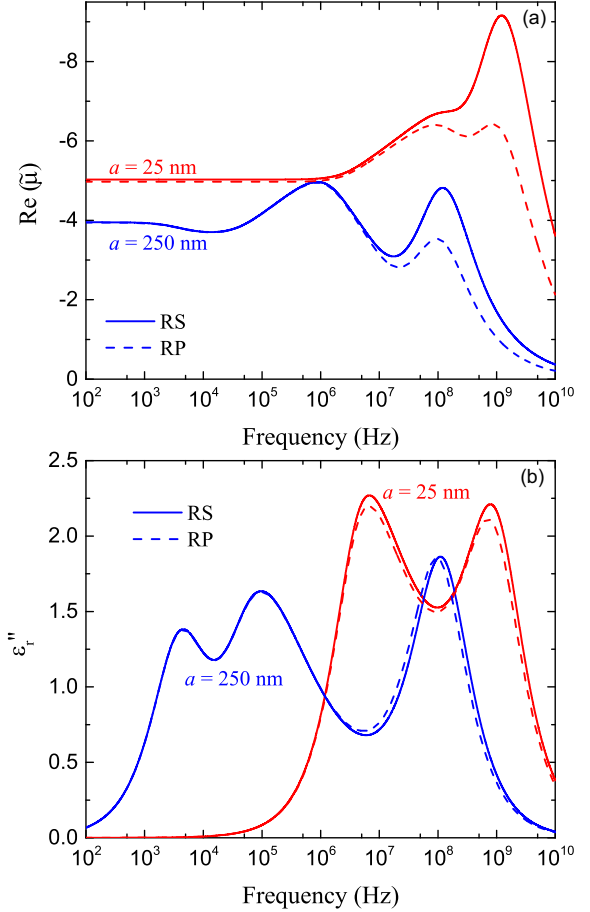


FIG. 7. Real part of the dimensionless dynamic electrophoretic mobility $\tilde{\mu}$ (a), and imaginary part of the relative permittivity ϵ_r'' (b), as a function of the field frequency. Particle radii in nm as indicated. Data: $\phi = 0.01$, $c^{\text{max}} = 4.0 \text{ mol/L}$, $\sigma = -30 \mu\text{C}/\text{cm}^2$. Solid lines: RS model; dashed lines: RP model.

with radius. In addition, the MWO relaxations are shifted to lower frequencies the larger the size, and the same happens to the inertial relaxation.

In addition, in Fig. 7 we present a different study: the real part of the dimensionless electrophoretic mobility [Fig. 7(a)] and the imaginary part of the relative permittivity of the colloid [Fig. 7(b)] are plotted as a function of the frequency of the alternating electric field for two particle radii: 25 and 250 nm, maximum concentration of species $c^{\text{max}} = 4.0 \text{ mol/L}$ (effective diameter $2R = 0.75 \text{ nm}$), particle volume fraction $\phi = 0.01$, and surface charge density $\sigma = -30.0 \mu\text{C}/\text{cm}^2$. This representation is intended to stress the low-frequency processes occurring in the EDL, to which the permittivity is known to be extremely sensitive, while dynamic mobility responds rather to high-frequency fields, producing MW relaxations, and eventually inertial decay [see, for example, Fig. 3(a)] [71,72].

One of the most important features that can be observed in Fig. 7(a) is that as particle radius increases, the relative influence of finite-size effects on the mobility decreases as one could expect, although there is an important contribution at high frequencies that corresponds to the relaxation of the MW-process associated to the counterion condensation region

[compare between solid lines (full model RS) and dashed lines (RP model)], at each particle radius. However, the imaginary part of the permittivity of the colloid in Fig. 7(b), is rather insensitive to the consideration of finite-size effects, as we obtain practically the same results with RS and RP approaches.

What is really different as particle radius increases is the presence of the α -relaxation process (lowest frequency peak of ε_r''), only observable in colloids in salt solutions or even in realistic salt-free colloids, mainly for large particles. For frequencies below the one characteristic of this process, concentration polarization clouds of neutral electrolyte are produced on each side of the particle in the presence of the electric field. For negative particles, with EDL enriched in cations, these will be accumulated by the field (assumed pointing from left to right) on the right hand side of the particle, and will add to the anions transported from the bulk, and accumulated in the same region. As a result, the concentration of both cations and anions will be increased on the right side, and by a similar mechanism, they will be depleted on the left. This opposes the MWO polarization and hence increases the particle speed. When the α -relaxation frequency is reached, this phenomenon cannot take place and the mobility decreases. Strictly, the α relaxation process is impeded in pure salt-free colloids, as there is no way for the concentration polarization phenomenon to be built because of the absence of the above described gradient of neutral salt, an essential requirement for the α process to be developed [2]. In contrast, it has been shown that the α -relaxation process may be present in realistic salt-free colloids. The reason lays on the fact that a realistic salt-free colloid behaves like a colloid in a low salt solution [60], with not only counterions but also coions in the solution, which are essential for the generation of the concentration polarization phenomenon of the α -process. For the mobility representation in Fig. 7(a), and for the largest radius, the α -process provokes the above mentioned decrease of the mobility at low frequencies when it is relaxed. Recall that in many situations of large particle radius, the lowest frequency MW-process (the MWO process; second peak of ε_r'' for the case $a = 250$ nm as frequency increases in Fig. 7(b)) normally brakes the particle motion. As mentioned before, the decrease of the mobility as frequency is further increased after the MWO relaxation process, is due to the inertia. At higher frequencies, the second MW-relaxation process (highest frequency peak of ε_r'' in Fig. 7(b), that corresponds to the counterions condensate, relaxes raising the mobility again. At even larger frequencies, the inertia finally leads the mobility toward zero.

E. Finite-size effects and particle surface charge

The particle surface charge is a crucial parameter for the present study, as, to begin with, for sufficiently high charge values the ionic condensation phenomenon takes place [38]. Furthermore, as the particle charge increases, so does the mobility, until the condensation phenomenon starts to control the dynamic response. For larger particle charges, the condensate region is simply fed with additional counterions whereas the double layer hardly changes. An effective particle charge seems to control the mobility, that remains nearly constant for

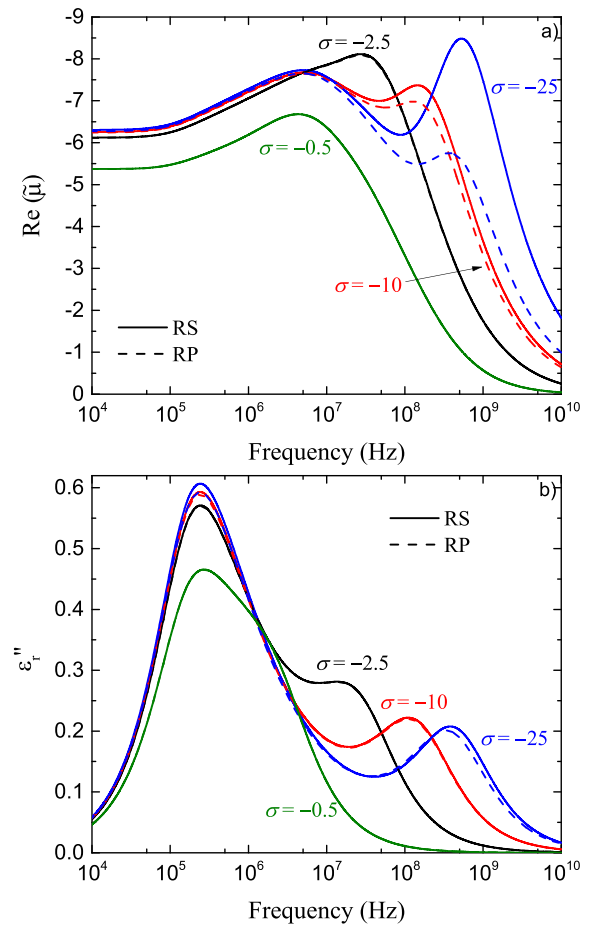


FIG. 8. Real part of the dimensionless dynamic electrophoretic mobility $\tilde{\mu}$ (a), and imaginary part of the relative permittivity ε_r'' (b), as a function of the field frequency. Particle surface charge density in $\mu\text{C}/\text{cm}^2$ as indicated. Data: $\phi = 0.001$, $c^{\text{max}} = 2.5$ mol/L, $a = 50$ nm. Solid lines: RS model; dashed lines: RP model.

even larger particle charges beyond the onset for the counterion condensation. The description of this condensation region populated with counterions is very sensitive to the consideration of whether the counterions in it have finite size or not, as discussed above.

To explore this hypothesis, in the present section different particle surface charges will be studied, always comparing, for brevity, RS and RP models only. The ion size in the former ($2R = 0.87$ nm) corresponds to a maximum concentration of species in the condensate of $c^{\text{max}} = 2.5$ mol/L. Thus, in Fig. 8 the real part of the dimensionless electrophoretic mobility [Fig. 8(a)] and the imaginary part of the relative permittivity [Fig. 8(b)] are shown for different particle surface charge densities σ up to the values where the counterion condensation is expected to occur. For such reason we explore σ values of -0.5 , -2.5 , -10.0 , and -25.0 $\mu\text{C}/\text{cm}^2$ in Fig. 8. In all cases, the particle volume fraction is $\phi = 0.001$, and the particle radius $a = 50$ nm.

For the lowest surface charge in Fig. 8, dashed lines (RP model) are almost indistinguishable from the solid lines used to represent the full realistic predictions (RS model). As surface charge increases, the MWO and the condensate MW

relaxation processes start to separate. Note that for the conditions chosen in Fig. 8, the α -relaxation process is absent. If the particle charge is further increased, then two relevant facts are clearly displayed. The first one deals with the saturation of the low frequency mobility and the practical invariance of the lowest frequency relaxation process [the MWO one, first global peak of ε_r'' in Fig. 8(b)] once the particle charge reaches the onset for the condensation. Raising the charge has the only consequence of accumulating more counterions in the condensate, whereas the double layer remains essentially unaffected. The second aspect has to do with the fact that finite-size effects confine their importance to the condensate region once its population of counterions is high enough. Note that a second maximum in mobility starts to grow with the increase in particle charge while shifting to larger frequencies. This is confirmed by the dielectric dispersion predictions [Fig. 8(b)], where one can observe that the MW-relaxation of the condensate (second peak in ε_r'') is separated from that of the diffuse layer, and moves toward larger frequencies the larger the particle charge. In the literature of ideal salt-free colloids, such shift has been correlated with the increase in the conductivity of the condensate layer as it gets more populated in counterions due to the rise of surface charge density. The same explanation can be applied in the present realistic salt-free case, because the key factor is the counterion condensation layer. In summary, realistic size effects have an outstanding influence on the high frequency mobility of highly charged particles.

V. CONCLUSIONS

With the intention of progressively approaching the realistic conditions of colloids in aqueous solutions, several theoretical aspects have been dealt with in this work, always related to the so-called salt-free systems. Although such systems have been previously explored theoretically, those studies have been limited to specific situations, namely, dilute, pure, or ideal salt-free colloids (pointlike counterions as the only ionic species) [73–75]; concentrated systems in the same conditions [3,23,76]; inclusion of ion size effects in pure salt-free systems [28,77]; realistic chemistry of the solution (water dissociation, CO₂ contamination [20,33,78]). The present work means an advance over all previous approaches, by including in a single general model all the features mentioned, which are particular cases of the theoretical treatment proposed.

Specifically, we present a complete theoretical electrokinetic model which allows to predict the complex dynamic electrophoretic mobility and complex relative permittivity of a realistic aqueous nanocolloid in the presence of an alternating electric field. We have considered for the first time colloids of arbitrary concentration, finite-size effects for chemical species, and a realistic chemistry for the solution where the colloidal particles are immersed. This has been done by jointly applying a mean-field cell model for particle concentration effects, and a nonequilibrium scenario accounting for association-dissociation processes in the chemical reactions, including nonidealities linked to the finiteness of the size of the species in solution.

It has been found that, depending on the frequency of the applied electric field, finite-size effects in realistic salt-free colloids cannot be dismissed. At low frequencies and for low to moderate particle volume fractions, the realistic pointlike approach can be considered as a good approximation to the full model developed in this work for most of the cases analyzed upon varying particle surface charge density or particle radius. In contrast, finite-size considerations are essential to get a proper description of the high frequency mobility response, provided that the particle surface charge is high.

Also, the counterion condensation phenomenon that develops in a region very close to the particles surface is clearly better described when the finite size of species is accounted for, which might have important implications in the understanding of the self-assembly of bionanomaterials or in the compaction of genetic material [38,79,80].

In the future, appropriate electrokinetic experiments with realistic colloids have to be carefully designed to check and quantify the role of a potentially essential feature such as the finite size of chemical species for the development of nanofluidic devices [81]. In addition, a generalization of the model for realistic electrolyte solutions of arbitrary ionic strength would be desirable.

ACKNOWLEDGMENTS

This study has been partially financed by the Consejería de Conocimiento, Investigación y Universidad, Junta de Andalucía and European Regional Development Fund (ERDF), Reference No. SOMM17/6105/UGR,B-FQM-141-UGR18, and Ministerio de Ciencia, Innovación y Universidades, Spain (Grant No. PGC2018-098770-B-I00).

-
- [1] J. Lyklema, *Fundamentals of Interface and Colloid Science*, Vol. 2 (Academic Press, London, 1995).
- [2] V. Shilov, A. Delgado, F. González-Caballero, J. Horro, J. López-García, and C. Grosse, Polarization of the electrical double layer: Time evolution after application of an electric field, *J. Colloid Interface Sci.* **232**, 141 (2000).
- [3] H. Ohshima, *Electrical Phenomena at Interfaces and Biointerfaces: Fundamentals and Applications in Nano-, Bio-, and Environmental Sciences* (John Wiley & Sons, New Jersey, 2012).

- [4] J. Merlin and J. F. Duval, Electrodynamics of soft multilayered particles dispersions: Dielectric permittivity and dynamic mobility, *Phys. Chem. Chem. Phys.* **16**, 15173 (2014).
- [5] M. López-Viata, M. M. El-Hammadi, L. Cabeza, J. Prados, C. Melguizo, M. A. Ruiz Martínez, J. L. Arias, and Á. V. Delgado, Development and characterization of magnetite/poly(butylcyanoacrylate) nanoparticles for magnetic targeted delivery of cancer drugs, *AAPS PharmSciTech* **18**, 3042 (2017).

- [6] Z. Adamczyk, M. Morga, D. Kosior, and P. Batys, Conformations of poly-L-lysine molecules in electrolyte solutions: Modeling and experimental measurements, *J. Phys. Chem. C* **122**, 23180 (2018).
- [7] M. Dabkowska, M. Adamczak, J. Barbasz, M. Ciesla, and B. Machalinski, Adsorption/desorption transition of recombinant human neurotrophin 4: Physicochemical characterization, *Langmuir* **33**, 9548 (2017).
- [8] A. Mondal and G. C. Shit, Transport of magneto-nanoparticles during electro-osmotic flow in a micro-tube in the presence of magnetic field for drug delivery application, *J. Magn. Magn. Mater.* **442**, 319 (2017).
- [9] J. Varshosaz, E. Khabbazian, F. Hassanzadeh, H. Sadeghi Aliabadi, M. Rostami, and S. Taymouri, Synthesis of biotin-targeted chitosan/poly (methyl vinyl ether-alt-maleic acid) copolymeric micelles for delivery of doxorubicin, *IET Nanobiotechnol.* **11**, 843 (2017).
- [10] N. Welsch, A. L. Becker, J. Dzubiella, and M. Ballauff, Core-shell microgels as “smart” carriers for enzymes, *Soft Matter* **8**, 1428 (2012).
- [11] J. F. Duval, C. Werner, and R. Zimmermann, Electrokinetics of soft polymeric interphases with layered distribution of anionic and cationic charges, *Current Opin. Colloid Interface Sci.* **24**, 1 (2016).
- [12] R. Ni, D. Cao, and W. Wang, A Monte Carlo study of spherical electrical double layer of macroions-polyelectrolytes systems in salt-free solutions, *J. Phys. Chem. B* **110**, 26232 (2006).
- [13] T. Y. Wang, Y. J. Sheng, and H. K. Tsao, Donnan potential of dilute colloidal dispersions: Monte Carlo simulations, *J. Colloid Interface Sci.* **340**, 192 (2009).
- [14] T. Y. Wang, H. T. Li, Y. J. Sheng, and H. K. Tsao, Equilibrium sedimentation profile of dilute, salt-free charged colloids, *J. Chem. Phys.* **129**, 204504 (2008).
- [15] Y. A. Budkov, A. I. Frolov, M. G. Kiselev, and N. V. Brilliantov, Surface-induced liquid-gas transition in salt-free solutions of model charged colloids, *J. Chem. Phys.* **139**, 194901 (2013).
- [16] T. Palberg, Crystallization kinetics of colloidal model suspensions: Recent achievements and new perspectives, *J. Phys.: Condens. Matter* **26**, 333101 (2014).
- [17] E. K. Zholkovskij, J. H. Masliyah, V. N. Shilov, and S. Bhattachalge, Electrokinetic phenomena in concentrated disperse systems: General problem formulation and spherical cell approach, *Adv. Colloid Interface Sci.* **134-35**, 279 (2007).
- [18] R. W. O'Brien, B. R. Midmore, A. Lamb, and R. J. Hunter, Electroacoustic studies of moderately concentrated colloidal suspensions, *Faraday Discuss. Chem. Soc.* **90**, 301 (1990).
- [19] J. M. Ding and H. J. Keh, The electrophoretic mobility and electric conductivity of a concentrated suspension of colloidal spheres with arbitrary double-layer thickness, *J. Colloid Interface Sci.* **236**, 180 (2001).
- [20] A. V. Delgado, F. Carrique, R. Roa, and E. Ruiz-Reina, Recent developments in electrokinetics of salt-free concentrated suspensions, *Curr. Opin. Colloid Interface Sci.* **24**, 32 (2016).
- [21] J. G. Ibarra-Armenta, A. Martín-Molina, and M. Quesada-Pérez, Testing a modified model of the Poisson-Boltzmann theory that includes ion size effects through Monte Carlo simulations, *Phys. Chem. Chem. Phys.* **11**, 309 (2009).
- [22] R. O'Brien, A. Jones, and W. Rowlands, A new formula for the dynamic mobility in a concentrated colloid, *Colloids Surf. A* **218**, 89 (2003).
- [23] F. Carrique, E. Ruiz-Reina, F. J. Arroyo, M. Jiménez, and A. V. Delgado, Dielectric response of a concentrated colloidal suspension in a salt-free medium, *Langmuir* **24**, 11544 (2008).
- [24] A. Dukhin, V. Shilov, H. Ohshima, and P. Goetz, Electroacoustic phenomena in concentrated dispersions: New theory and cvi experiment, *Langmuir* **15**, 6692 (1999).
- [25] J. J. Lopez-Garcia, C. Grosse, and J. Horno, Numerical calculation of the electrophoretic mobility of concentrated suspensions of soft particles, *J. Colloid Interface Sci.* **301**, 651 (2006).
- [26] Y. Y. He and E. Lee, Electrophoresis in concentrated dispersions of charged porous spheres, *Chem. Eng. Sci.* **63**, 5719 (2008).
- [27] F. Carrique, E. Ruiz-Reina, R. Roa, F. J. Arroyo, and A. V. Delgado, General electrokinetic model for concentrated suspensions in aqueous electrolyte solutions: Electrophoretic mobility and electrical conductivity in static electric fields, *J. Colloid Interface Sci.* **455**, 46 (2015).
- [28] R. Roa, F. Carrique, and E. Ruiz-Reina, Ion size effects on the electrokinetics of salt-free concentrated suspensions in ac fields, *J. Colloid Interface Sci.* **387**, 153 (2012).
- [29] J. J. Lopez-Garcia, J. Horno, and C. Grosse, Differential capacitance of the diffuse double layer at electrode-electrolyte interfaces considering ions as dielectric spheres: Part I. Binary electrolyte solutions, *J. Colloid Interface Sci.* **496**, 531 (2017).
- [30] S. Mukherjee, P. Goswami, J. Dhar, S. Dasgupta, and S. Chakraborty, Ion-size dependent electroosmosis of viscoelastic fluids in microfluidic channels with interfacial slip, *Phys. Fluids* **29**, 072002 (2017).
- [31] H. Ohshima, Ion size effect on counterion condensation around a spherical colloidal particle in a salt-free medium containing only counterions, *Colloid Polym. Sci.* **296**, 1293 (2018).
- [32] J. S. Sin and U. H. Kim, Ion size effect on electrostatic and electroosmotic properties in soft nanochannels with ph-dependent charge density, *Phys. Chem. Chem. Phys.* **20**, 22961 (2018).
- [33] F. Carrique, E. Ruiz-Reina, L. Lechuga, F. J. Arroyo, and A. V. Delgado, Effects of non-equilibrium association-dissociation processes in the dynamic electrophoretic mobility and dielectric response of realistic salt-free concentrated suspensions, *Adv. Colloid Interface Sci.* **201**, 57 (2013).
- [34] A. R. Denton, Poisson-Boltzmann theory of charged colloids: limits of the cell model for salty suspensions, *J. Phys.: Condens. Matter* **22**, 364108 (2010).
- [35] J. Dobnikar, R. Castañeda Priego, H. Von Grünberg, and E. Trizac, Testing the relevance of effective interaction potentials between highly charged colloids in suspension, *New J. Phys.* **8**, 277 (2006).
- [36] Y. Hallez, J. Diatta, and M. Meireles, Quantitative assessment of the accuracy of the Poisson-Boltzmann cell model for salty suspensions, *Langmuir* **30**, 6721 (2014).
- [37] J. J. López-García, M. J. Aranda-Rascón, C. Grosse, and J. Horno, Equilibrium electric double layer of charged spherical colloidal particles: Effect of different distances of minimum ion approach to the particle surface, *J. Phys. Chem. B* **114**, 7548 (2010).
- [38] D. A. J. Gillespie, J. E. Hallett, O. Elujoba, A. F. Che Hamzah, R. M. Richardson, and P. Bartlett, Counterion condensation on spheres in the salt-free limit, *Soft Matter* **10**, 566 (2014).
- [39] A. Chatterji and J. Horbach, The role of effective charges in the electrophoresis of highly charged colloids, *J. Phys.: Condens. Matter* **22**, 494102 (2010).

- [40] G. Tellez, Nonlinear screening of charged macromolecules, *Philos. Trans. R. Soc. A* **369**, 322 (2011).
- [41] G. S. Manning, A counterion condensation theory for the relaxation, rise, and frequency dependence of the parallel polarization of rodlike polyelectrolytes, *Eur. Phys. J. E* **34**, 39 (2011).
- [42] I. Adroher-Benitez, S. Ahualli, D. Bastos-Gonzalez, J. Ramos, J. Forcada, and A. Moncho-Jorda, The effect of electrosteric interactions on the effective charge of thermoresponsive ionic microgels: Theory and experiments, *J. Pol. Sci. B Pol. Phys.* **54**, 2038 (2016).
- [43] D. Botin, L. M. Mapa, H. Schweinfurth, B. Sieber, C. Wittenberg, and T. Palberg, An empirical correction for moderate multiple scattering in super-heterodyne light scattering, *J. Chem. Phys.* **146**, 204904 (2017).
- [44] S. Kuwabara, The forces experienced by randomly distributed parallel circular cylinders or spheres in a viscous flow at small reynolds numbers, *J. Phys. Soc. Jpn.* **14**, 527 (1959).
- [45] J. Bikerman, XXXIX. Structure and capacity of electrical double layer, *Philos. Mag.* **33**, 384 (1942).
- [46] N. F. Carnahan and K. E. Starling, Equation of state for nonattracting rigid spheres, *J. Chem. Phys.* **51**, 635 (1969).
- [47] T. Boublik, Hard-sphere equation of state, *J. Chem. Phys.* **53**, 471 (1970).
- [48] G. A. Mansoori, N. F. Carnahan, K. E. Starling, and T. W. Leland, Equilibrium thermodynamics properties of the mixture of hard spheres, *J. Chem. Phys.* **54**, 1523 (1971).
- [49] H. Ohshima, An approximate analytic solution to the modified Poisson-Boltzmann equation: effects of ionic size, *Colloid Polym. Sci.* **294**, 2121 (2016).
- [50] J. J. López-García, J. Horno, and C. Grosse, Influence of steric interactions on the dielectric and electrokinetic properties in colloidal suspensions, *J. Colloid Interface Sci.* **458**, 273 (2015).
- [51] M. L. Jiménez, S. Ahualli, P. Arenas-Guerrero, M. M. Fernández, G. Iglesias, and A. V. Delgado, Multiionic effects on the capacitance of porous electrodes, *Phys. Chem. Chem. Phys.* **20**, 5012 (2018).
- [52] J. J. López-García, J. Horno, and C. Grosse, Ion size effects on the dielectric and electrokinetic properties in aqueous colloidal suspensions, *Curr. Opin. Colloid Interface Sci.* **24**, 23 (2016).
- [53] I. Borukhov, D. Andelman, and H. Orland, Steric Effects in Electrolytes: A Modified Poisson-Boltzmann Equation, *Phys. Rev. Lett.* **79**, 435 (1997).
- [54] See Supplemental Material at <http://link.aps.org/supplemental/10.1103/PhysRevE.102.032614> for details of derivations not included in the main text, specifically, obtaining ion and neutral species concentration, solving the modified PB equation, perturbation scheme for electrokinetic equations, derivations of the dynamic mobility, and dielectric permittivity of the colloid.
- [55] R. Roa, F. Carrique, and E. Ruiz-Reina, Ion size effects on the electric double layer of a spherical particle in a realistic salt-free concentrated suspension, *Phys. Chem. Chem. Phys.* **13**, 9644 (2011).
- [56] I. S. Butler and J. F. Harrod, *Inorganic Chemistry: Principles and Applications* (Benjamin-Cummings, New York, 1989).
- [57] N. Greenwood and A. Earnshaw, *Chemistry of the Elements*, 2nd ed. (Butterworth-Heinemann, Oxford, UK, 1997).
- [58] M. Soustelle, *An Introduction to Chemical Kinetics*, ISTE (John Wiley & Sons, New Jersey, 2013).
- [59] J. Baygents and D. Saville, Electrophoresis of small particles and fluid globules in weak electrolytes, *J. Colloid Interface Sci.* **146**, 9 (1991).
- [60] F. Carrique, E. Ruiz-Reina, F. J. Arroyo, and A. V. Delgado, Dynamic electrophoretic mobility of spherical colloidal particles in realistic aqueous salt-free concentrated suspensions, *J. Phys. Chem. B* **114**, 6134 (2010).
- [61] R. O'Brien, D. Cannon, and W. Rowlands, Electroacoustic determination of particle size and zeta potential, *J. Colloid Interface Sci.* **173**, 406 (1995).
- [62] Y. Marcus, Ionic radii in aqueous solutions, *Chem. Rev.* **88**, 1475 (1988).
- [63] J. J. López-García and J. Horno, Poisson-Boltzmann description of the electrical double layer including ion size effects, *Langmuir* **27**, 13970 (2011).
- [64] M. L. Jiménez, M. M. Fernández, S. Ahualli, G. Iglesias, and A. V. Delgado, Predictions of the maximum energy extracted from salinity exchange inside porous electrodes, *J. Colloid Interface Sci.* **402**, 340 (2013).
- [65] T. Bellini, F. Mantegazza, V. Degiorgio, R. Avallone, and D. A. Saville, Electric Polarizability of Polyelectrolytes: Maxwell-Wagner and Electrokinetic Relaxation, *Phys. Rev. Lett.* **82**, 5160 (1999).
- [66] P. Arenas-Guerrero, S. Ahualli, A. V. Delgado, and M. L. Jiménez, Electric birefringence of gold nanorods: Effect of surfactant coating, *J. Phys. Chem. C* **123**, 26623 (2019).
- [67] H. Ohshima, Electrophoretic mobility of a spherical colloidal particle in a salt-free medium, *J. Colloid Interface Sci.* **248**, 499 (2002).
- [68] M. Medebach and T. Palberg, Phenomenology of colloidal crystal electrophoresis, *J. Chem. Phys.* **119**, 3360 (2003).
- [69] V. Lobaskin, B. Dünweg, M. Medebach, T. Palberg, and C. Holm, Electrophoresis of Colloidal Dispersions in the Low-Salt Regime, *Phys. Rev. Lett.* **98**, 176105 (2007).
- [70] P. Wiersema, A. Loeb, and J. T. G. Overbeek, Calculation of the electrophoretic mobility of a spherical colloid particle, *J. Colloid Interface Sci.* **22**, 78 (1966).
- [71] Á. V. Delgado, *Interfacial Electrokinetics and Electrophoresis*, Vol. 106 (CRC Press, Boca Raton, FL, 2001).
- [72] F. Carrique, E. Ruiz-Reina, R. Roa, F. J. Arroyo, and Á. V. Delgado, Ionic coupling effects in dynamic electrophoresis and electric permittivity of aqueous concentrated suspensions, *Colloids Surf. A* **541**, 195 (2018).
- [73] J. Lyklema, *Fundamentals of Interface and Colloid Science: Soft Colloids*, Vol. 5 (Elsevier, Amsterdam, 2005).
- [74] G. S. Manning, Counterion condensation on charged spheres, cylinders, and planes, *J. Phys. Chem. B* **111**, 8554 (2007).
- [75] H. Ohshima, Electrokinetic phenomena in a dilute suspension of spherical colloidal particles in a salt-free medium, *Colloids Surf. A* **222**, 207 (2003).
- [76] F. Carrique, E. Ruiz-Reina, F. J. Arroyo, and Á. V. Delgado, Cell model of the direct current electrokinetics in salt-free concentrated suspensions: The role of boundary conditions, *J. Phys. Chem. B* **110**, 18313 (2006).
- [77] R. Roa, F. Carrique, and E. Ruiz-Reina, dc electrokinetics for spherical particles in salt-free concentrated suspensions including ion size effects, *Phys. Chem. Chem. Phys.* **13**, 19437 (2011).

- [78] E. Ruiz-Reina, F. Carrique, and L. Lechuga, Dc electrophoresis and viscosity of realistic salt-free concentrated suspensions: Non-equilibrium dissociation-association processes, *J. Colloid Interface Sci.* **417**, 60 (2014).
- [79] R. K. Mishra, S. K. Ha, K. Verma, and S. K. Tiwari, Recent progress in selected bio-nanomaterials and their engineering applications: An overview, *J. Sci.: Adv. Mater. Devices* **3**, 263 (2018).
- [80] C. Gong, S. Sun, Y. Zhang, L. Sun, Z. Su, A. Wu, and G. Wei, Hierarchical nanomaterials via biomolecular self-assembly and bioinspiration for energy and environmental applications, *Nanoscale* **11**, 4147 (2019).
- [81] J. Hoffmann and D. Gillespie, Ion correlations in nanofluidic channels: Effects of ion size, valence, and concentration on voltage- and pressure-driven currents, *Langmuir* **29**, 1303 (2013).